analytical chemistry

pubs.acs.org/ac
Article

Exploiting Flavylium Merocyanine Dyes for Intrinsic, Multiplexed Labeling of the Endoplasmic Reticulum

Quintashia D. Wilson, Helen H. Lin, Eric Y. Lin, Lin-Jiun Chen, and Ellen M. Sletten*

Cite This: *Anal. Chem.* 2025, 97, 5595−5604
Read Online

ABSTRACT: Merocyanine dyes are a versatile class of donor−acceptor polymethine dyes that exhibit unique properties depending on their structural makeup and surrounding environment. Scaffolds that favor the cyanine state (*i.e.*, narrow, red-shifted absorption and high fluorescence quantum yields) in biologically relevant settings are highly advantageous for multiplexed labeling experiments, but remain limited by their visible absorption. Herein, we synthesize a new class of far-red (650−700 nm) to near-infrared (NIR, 700−1000 nm) flavylium merocyanine dyes and demonstrate that, unlike conventional scaffolds, they favor the cyanine state with increasing solvent viscosity and hydrogen bond donation, rather than polarity. We leverage these advantageous properties for live cell labeling, where we observed intrinsic targeting to the endoplasmic reticulum (ER) and lipid droplets, and minimal crosstalk with commercial stains. We reveal that intrinsic ER labeling is achieved by the dipolarity in the cyanine state and lipophilicity (Clog*P*) of the merocyanine architecture, making this class of dyes a simple, red-shifted alternative to the more structurally complex ER stains currently available.

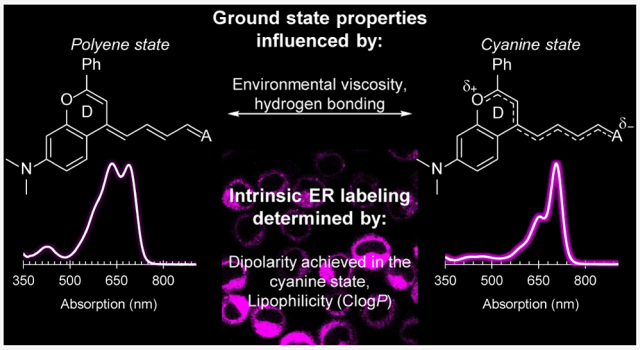

INTRODUCTION

A hallmark of optical imaging is the ease of multiplexing, which enables the simultaneous observation of distinct biological structures and processes in living cells.[1] Key to these experiments is the selection of fluorophores with good spectral separation to minimize crosstalk. The landscape of commercial cell stains is extensive, but primarily skewed to absorption wavelengths ($\lambda_{max,abs}$) between 400 and 650 nm, increasing the likelihood of spectral overlap. Furthermore, these wavelengths are not amenable to complex biological settings (*e.g.*, organoids and whole animals) due to poor tissue penetration and high background fluorescence.[2] As such, the development of fluorophores that absorb beyond 650 nm is crucial to the optimization and translation of these technologies.

Among the different classes of small molecule fluorophores, polymethine dyes are an ideal scaffold for far-red (650−700 nm) and near-infrared (NIR, 700−1000 nm) imaging, as their structural makeup (an extendable polymethine chain flanked by two end groups) permits easy access to these advantageous wavelengths.[3−9] The most ubiquitous polymethine scaffolds for cell labeling are cationic dyes (*e.g.*, Cy5 and its derivatives), which feature a positive charge distributed between two electron-donating end groups.[10] In low polarity solvents, the "cyanine" ground state is favored, where the positive charge is fully delocalized across the entire molecule, and there is minimal bond-length alternation (BLA) in the polymethine chain (Figure 1A).[11−13] This results in a red-shifted absorption band with a small full-width half-maximum (FWHM) and good fluorescence quantum yield (ϕ_F).[14,15] These properties are highly advantageous for multiplexed imaging, but harder to achieve in biological settings due to H-aggregation and ground state desymmetrization.[16−19] Most cationic dyes are insoluble in biological media, forming broad, blue-shifted H-aggregates that are nonemissive.[16−20] Even when soluble, aqueous environments preferentially stabilize the asymmetric "polyene" ground state, where the charge is localized on either end group and there is considerable BLA in the polymethine chain.[21−23] As a result, cationic polymethine dyes often exhibit broad, blue-shifted absorption bands and diminished ϕ_F in biological settings. Many clever strategies have emerged to alleviate this problem,[13,17−25] but require additional functionalization steps and/or formulations that could affect cell labeling properties.

To avoid these limitations, we are interested in exploring the neutral merocyanine scaffold. Like cationic polymethine dyes, merocyanine dyes also exist between a polyene and cyanine ground state (Figure 1A).[12,14] However, because they

Received: November 15, 2024
Revised: February 2, 2025
Accepted: February 23, 2025
Published: March 4, 2025

https://doi.org/10.1021/acs.analchem.4c06185
Anal. Chem. 2025, 97, 5595−5604

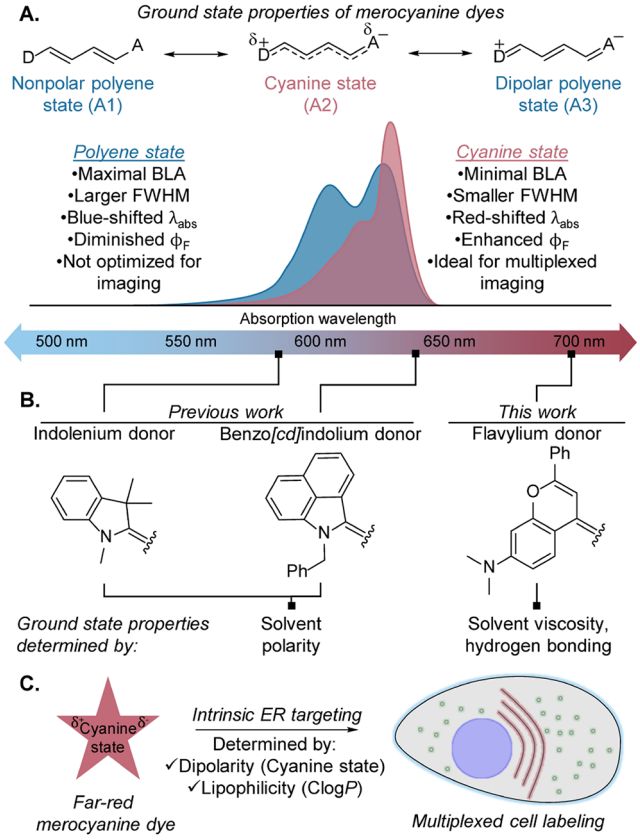

Figure 1. Overiew of merocyanine dyes. (A) Characteristics of merocyanine ground states, including bond-length alternation (BLA), full-width half-maximum (FWHM), absorption wavelength (λ_{abs}) and fluorescence quantum yield (ϕ_F) properties. (B) Absorption wavelengths and ground state properties of merocyanine dyes with different donors and the same acceptor. (C) Requirements for intrinsic labeling of the endoplasmic reticulum of merocyanine dyes developed in this work.

contain one electron-donating and one electron-accepting end group, merocyanine dyes exhibit two distinct polyene states that heavily depend on the strength of the donor−acceptor pair and solvent polarity.[26−31] We believe that merocyanine dyes between the nonpolar polyene (A1) and cyanine (A2) ground states have remarkable potential for biological imaging, as they exhibit increasing cyanine character with increasing environmental polarity.[32−37] Additionally, the inherent dipolarity of merocyanine dyes may impart unique cell localization properties from cationic dyes that are advantageous for cell labeling. Unfortunately, existing merocyanine scaffolds between the A1—A2 ground states (*e.g.*, dyes with indolenium and benzo[*cd*]indolium donors, Figure 1B) all absorb below 650 nm, stifling their capacity for multiplexing with commercial stains. Therefore, the goal of this work was to design a new class of red-shifted merocyanine dyes that favor the cyanine state under biologically relevant conditions, and examine their utility for cell labeling.

Toward this end, we selected the dimethylamino-substituted flavylium heterocycle as the donor end group, based on our previous success with red-shifted cationic polymethine dyes.[38,39] Furthermore, we hypothesized that its weak electron-donating properties would favor the desired A1—A2 ground states, leading to enhanced properties in biological conditions. Herein, we report a new class of flavylium merocyanine dyes that exist between the A1—A2 ground states, with absorption near or above 650 nm (Figure 1B). We evaluate their electronic ground states across a range of solvents to demonstrate that these dyes favor the cyanine state with increasing solvent viscosity and hydrogen bond donation, rather than polarity, which is canonically thought to determine the ground states of merocyanine dyes. We also examine their fluorescent properties to reveal that the ϕ_F of flavylium merocyanine dyes increases with both solvent polarity and viscosity, making them well-suited for biological investigations. Finally, we exploit these properties for live cell multiplexed labeling experiments, observing excellent localization in the endoplasmic reticulum (ER) and lipid droplets, and negligible crosstalk with commercial stains for the nucleus, cell membrane, lysosomes and mitochondria (Figure 1C). We attribute the intrinsic ER labeling to the dipolarity and lipophilicity (Clog*P*) of the merocyanine architecture, substantially expanding the utility of this scaffold for cell imaging.

EXPERIMENTAL SECTION

Materials and Instruments. Chemical reagents were purchased from commercial suppliers and used without purification. Nuclear magnetic resonance (^{1}H NMR and ^{13}C NMR) spectra were taken on a Bruker AV500 spectrometer and processed with MestReNova software. High resolution mass spectrometry data were obtained on an Agilent 6545 Q-TOF mass spectrometer. Absorption spectra were collected on a JASCO V-770 or JASCO V-710 UV−visible/NIR spectrophotometer. Excitation and emission spectra were collected on a Horiba PTI QuantaMaster400 series fluorimeter. Excited state lifetime measurements were performed on a Horiba Fluorolog-QM Series fluorimeter equipped with a delta diode setup and 529 nm excitation laser. All absorption, emission, excitation and lifetime measurements were collected using a 1 cm quartz cuvette. Microscopy was performed with a Leica STELLARIS 5 confocal microscope using the 405, 488, 561, and 638 nm lasers and 63× oil objective lens, or a Lecia SP8 LIGHTNING confocal microscope using the 405, 488, 577, and 660 nm lasers and 100× oil objective lens.

Synthesis of MalonoFlav4. 7-(dimethylamino)-2-phenyl-4-((1*E*,3*E*)-4-(*N*-phenylacetamido)buta-1,3-dien-1-yl)-chromenylium tetrafluoroborate (**6**) (40 mg, 76 μmol, 1.0 equiv), malononitrile (**2**) (20 mg, 0.30 mmol, 4.0 equiv) and NaOAc (39 mg, 0.30 mmol, 4.0 equiv) were added to a dram vial equipped with a stir bar and fitted with a PTFE-lined cap. The solids were dissolved in Ac_2O (1.9 mL) and heated to 120 °C for 30 min. The mixture was cooled to rt and evaporated onto silica gel. The crude product was purified via flash chromatography, eluting with DCM. The crude product was washed with MeOH (3 × 5 mL) to afford **MalonoFlav4** as a bronze turquoise solid (19 mg, 53 μmol, 70%). R_F = 0.23 in DCM. ^{1}H NMR (500 MHz, CD_2Cl_2) δ 7.92 (s, 2H), 7.76−7.40 (m, 6H), 7.08 (s, 1H), 6.84−6.45 (m, 4H), 3.10 (s, 6H). ^{13}C NMR (126 MHz, CD_2Cl_2) δ 158.91, 155.04, 154.93, 153.71, 146.75, 141.98, 132.88, 130.98, 129.30, 125.93, 124.90, 120.63, 116.88, 114.79, 111.65, 110.16, 109.62, 100.76, 98.48, 98.42, 70.96, 40.37, 30.09. HRMS (ESI): calculated for $C_{24}H_{20}N_3O^+$ $[M]^+$, 366.1601; found, 366.1595.

Synthesis of IndaFlav4. (*E*)-*N*-(3-(1,3-dioxo-1,3-dihydro-2*H*-inden-2-ylidene)prop-1-en-1-yl)-*N*-phenylacetamide (**7**) (30 mg, 95 μmol, 1.0 equiv), 7-(dimethylamino)-4-

https://doi.org/10.1021/acs.analchem.4c06185
Anal. Chem. 2025, 97, 5595−5604

methyl-2-phenylchromenylium tetrafluoroborate (**1**) (50 mg, 0.14 mmol, 1.5 equiv) and NaOAc (23 mg, 0.28 mmol, 3.0 equiv) were added to a dram vial equipped with a stir bar and fitted with a PTFE-lined cap. The solids were dissolved in *n*-BuOH (0.95 mL) and the mixture was heated to 80 °C for 50 min. The mixture was cooled to rt and evaporated onto silica gel. The crude product was purified via flash chromatography, eluting with a DCM/EtOH gradient of 0% EtOH, 0.1% EtOH and 0.5% EtOH to afford **IndaFlav4** as a shiny turquoise solid (36 mg, 81 μmol, 85%). R_F = 0.33 in 40:1 DCM:MeOH. ^{1}H NMR (500 MHz, CD_2Cl_2) δ 7.94 (dt, *J* = 6.0, 1.8 Hz, 2H), 7.86−7.75 (m, 5H), 7.71−7.66 (m, 2H), 7.61−7.56 (m, 1H), 7.56−7.47 (m, 3H), 7.18 (s, 1H), 6.81−6.72 (m, 2H), 6.57 (d, *J* = 2.6 Hz, 1H), 3.10 (s, 6H). ^{13}C NMR (126 MHz, CD_2Cl_2) δ 191.03, 154.66, 153.17, 149.67, 145.10, 133.86, 133.66, 132.60, 130.43, 128.88, 125.46, 124.52, 122.86, 121.76, 121.62, 111.17, 110.10, 100.69, 98.11, 39.96, 29.68. HRMS (ESI): calculated for $C_{30}H_{24}NO_3^+$ $[M]^+$, 446.1751; found, 446.1783.

Synthesis of BarbiFlav4. (*E*)-*N*-(3-(1,3-dimethyl-2,4,6-trioxotetrahydropyrimidin-5(2*H*)-ylidene)prop-1-en-1-yl)-*N*-phenylacetamide (**8**) (50 mg, 0.15 mmol, 1.0 equiv) and 7-(dimethylamino)-4-methyl-2-phenylchromenylium tetrafluoroborate (**1**) (80 mg, 0.23 mmol, 1.5 equiv) were added to a dram vial equipped with a stir bar and fitted with a PTFE-lined cap. The solids were dissolved in pyridine (1.5 mL) and the mixture was heated to 70 °C for 50 min. The mixture was cooled to rt and evaporated onto silica gel. The crude product was purified via flash chromatography, eluting with 200:1 DCM:MeOH to afford **BarbiFlav4** as a shiny dark blue solid (50 mg, 0.11 mmol, 72%). R_F = 0.21 in 40:1 DCM:MeOH. ^{1}H NMR (500 MHz, CD_2Cl_2) δ 8.09 (d, *J* = 12.2 Hz, 1H), 7.97−7.87 (m, 4H), 7.74 (d, *J* = 9.2 Hz, 1H), 7.54−7.49 (m, 3H), 7.21 (s, 1H), 6.79−6.71 (m, 2H), 6.56 (d, *J* = 2.6 Hz, 1H), 3.29 (d, *J* = 1.9 Hz, 6H), 3.09 (s, 6H). ^{13}C NMR (126 MHz, CD_2Cl_2) δ 163.60, 162.74, 156.20, 155.31, 155.23, 153.81, 153.04, 152.43, 142.99, 132.75, 131.07, 129.31, 125.98, 125.14, 124.17, 111.85, 111.60, 110.54, 106.59, 101.16, 98.31, 40.37, 28.44, 28.40, 27.79. HRMS (ESI): calculated for $C_{27}H_{26}N_3O_4^+$ $[M]^+$, 456.1918; found, 456.1923.

RESULTS AND DISCUSSION

Design and Synthesis. We approached the design of red-shifted merocyanine dyes with the impression that the flavylium heterocycle (**1**) is a weak electron donor that would lie between the A1—A2 ground states with a well-matched acceptor (Scheme 1A). We selected malononitrile (**2**), 1,3-indandione (**3**) and *N*,*N*-1,3-dimethyl barbituric acid (**4**) as respectively weak, moderate and strong electron acceptors due to their commercial availability and prevalence in other merocyanine scaffolds (Scheme 1A).[26,40,41] Furthermore, we selected the tetramethine length, containing four methine units, for a balance of synthetic ease and red-shifted absorption. Synthesizing merocyanine dyes typically begins with the generation of an activated donor or acceptor hemicyanine dye that can undergo Knoevenagel condensation with a respective acceptor or donor group.[28] We envisioned that a donor hemicyanine dye based on **1** would be the most efficient way to access a panel of flavylium merocyanine dyes with varied acceptors (Scheme 1B). Refluxing **1** with malonaldehyde bis(phenylimine) (**5**) in a mixture of acetic acid and acetic anhydride readily afforded the desired donor hemicyanine dye **6** in 59% yield. Condensation of **6** with acceptor **2** occurred rapidly in the presence of base and heated acetic anhydride, generating the first merocyanine dye, named **MalonoFlav4**, in 70% yield. When we extended this procedure to acceptor **3**, a number of side products were observed, making the purification difficult. Instead, we decided to pursue acceptor hemicyanine dye **7**, which was synthesized by heating **3** with malonaldehyde linker **5** in acetic anhydride. Treatment of **7** with **1** in the presence of base and *n*-butanol afforded the second merocyanine dye, **IndaFlav4**, in 85% yield. We extended this methodology to barbituric acid acceptor **4** to generate hemicyanine dye **8**, which readily afforded the final merocyanine dye, **BarbiFlav4**, in 72% yield. We could also access **BarbiFlav4** from donor hemicyanine dye **6** (see S.I. synthetic procedures), demonstrating the versatility of merocyanine synthesis.

Scheme 1. Synthesis and Absorption Spectra of Flavylium Merocyanine Dyes. (A, B) Design and Synthesis of Flavylium Merocyanine Dyes Developed in This Work. (C) Normalized Absorption Spectra Showing the Ground State Properties of Flavylium Merocyanine Dyes with Increasing Polarity (IndaFlav4, 12 μM, in DCM vs DMSO) and Increasing Acceptor Strength (MalonoFlav4, 5.0 μM, vs BarbiFlav4, 12 μM, in DCM)

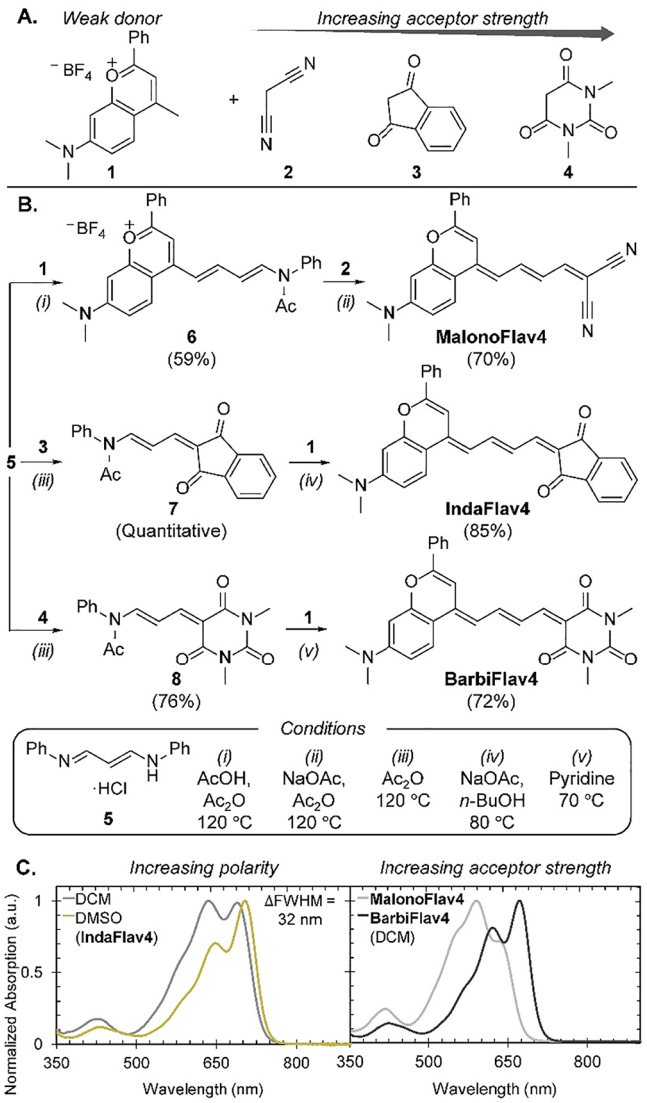

https://doi.org/10.1021/acs.analchem.4c06185
Anal. Chem. 2025, 97, 5595−5604

A.

Solvent	$\lambda_{max,\ abs}$ (nm)	FWHM (nm)	ϵ (M^{-1} cm^{-1})	$\lambda_{max,\ em}$ (nm)	ϕ_F (%)	$\epsilon \times \phi_F$ (M^{-1} cm^{-1})
DCM (*a*)	636, 689	145	31300 ± 200	737	1.8 ± 0.1	560 ± 30
1-Octanol (*b*)	701	105	44500 ± 400	723	10 ± 0.5	4500 ± 300
MeOH (*c*)	696	84	63000 ± 2000	732	4.9 ± 0.2	3100 ± 200
MeCN (*d*)	687	141	49000 ± 1000	720	3.3 ± 0.3	1600 ± 200
DMF (*e*)	697	122	37000 ± 500	738	5.7 ± 0.3	2100 ± 100
DMSO (*f*)	704	107	43000 ± 1000	731	16 ± 1	6900 ± 600
25% Water/MeCN (*g*)	697	89	37000 ± 1000	723	6.2 ± 0.4	2300 ± 200
25% Water/DMSO (*h*)	707	51	82000 ± 4000	731	15 ± 0.6	12000 ± 1000

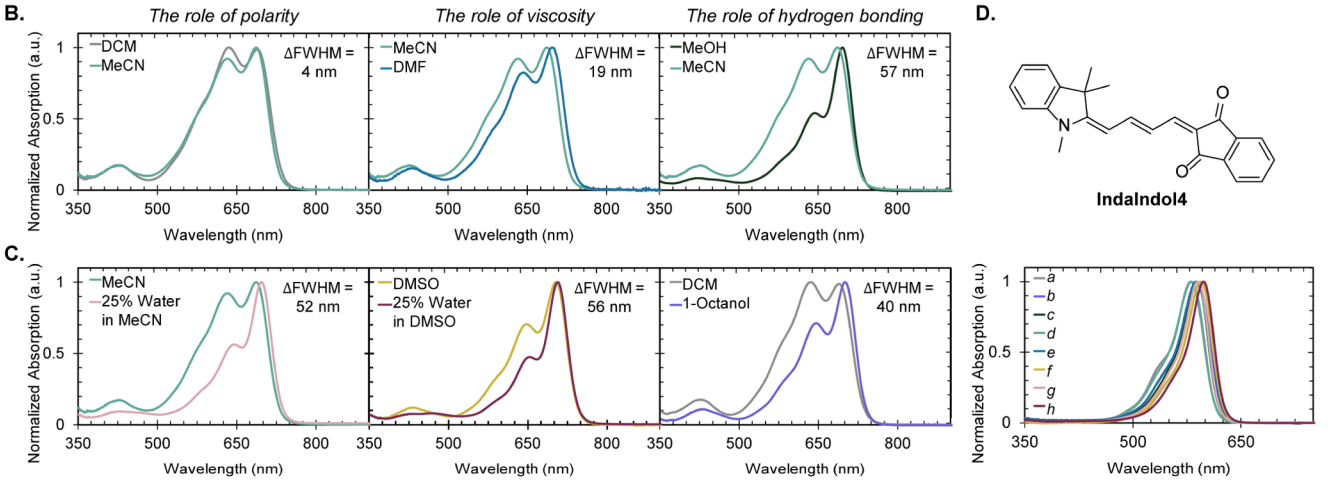

Figure 2. Absorption properties of **IndaFlav4** and **IndaIndol4** in various solvents. (A) Photophysical properties of **IndaFlav4** in various solvents. Normalized absorption spectra showing the change in full-width half-maximum (ΔFWHM) of **IndaFlav4** (12 μM) with (B) polarity (DCM vs MeCN), viscosity (MeCN vs DMF) and hydrogen bond donation (MeOH vs MeCN) and (C) solvent conditions with contributions from viscosity and hydrogen bond donation (MeCN vs 25% water/MeCN, DMSO vs 25% water/DMSO and DCM vs 1-octanol). (D) Structure and normalized absorption spectra of **IndaIndol4** (3.0 μM) in various solvents. Un-normalized spectra are reported in the Supporting Information (Figure S6).

With access to a panel of flavylium merocyanine dyes, we conducted a preliminary assessment of our design approach by evaluating the ground state properties of each dye in less polar dichloromethane (DCM) and more polar dimethyl sulfoxide (DMSO) (Scheme 1C and Figure S1A). Based on the large difference in their dielectric constants (ϵ_R = 9.08 vs 46.02) (Table S1), we expected to see stronger cyanine character in DMSO if the dyes exist between the A1—A2 states. For all three dyes, we observed a decrease in the FWHM (11−32 nm) and an increase in the red-shifted cyanine shoulder in DMSO, suggesting that they exist between the desired A1—A2 states. To verify that these results are not due to differences in solubility/H-aggregation, we collected absorption spectra in each solvent over a range of concentrations, and observed no spectral changes upon normalization (Figure S2A). Furthermore, we collected excitation spectra at the higher end of these concentrations (Figure S2B). In each case, the excitation spectra resemble their corresponding absorption spectra, supporting that the differences between DCM and DMSO reflect changes in the ground state, not aggregation. In addition to solvent polarity, there is also a noticeable correlation between cyanine character and acceptor strength (Scheme 1C), with **MalonoFlav4** favoring the polyene state and **BarbiFlav4** favoring the cyanine state. Beyond their ground state properties, all three merocyanine dyes possess remarkably red-shifted absorption (*ca.* 50−100 nm) compared to indolenium and benzo[*cd*]indolium tetramethine dyes with the same acceptors (Figure S3). We were especially delighted to see that **IndaFlav4** and**BarbiFlav4** absorb well above 650 nm, with **IndaFlav4** reaching the NIR region in DMSO. Overall, these results substantiate our hypothesis that the flavylium heterocycle is a weak electron donor capable of generating red-shifted merocyanine dyes that appear to favor the cyanine state with increasing solvent polarity.

Ground State Properties. Having performed a cursory assessment in DCM and DMSO, we proceeded to evaluate the ground states of these flavylium merocyanine dyes in methanol (MeOH) to gage how they perform in polar protic conditions (Figure S1B). We were unable to fully solubilize **MalonoFlav4** in MeOH, resulting in strong H-aggregation. Although the solubility improved in ethanol, we ultimately decided not to proceed with **MalonoFlav4** due to its limited solubility and weak emission across various solvents (Figure S4). In the case of **IndaFlav4** and **BarbiFlav4**, we were surprised to see that both dyes exhibit smaller FWHM in MeOH than DMSO, despite MeOH being a less polar solvent (ϵ_R = 32.63 vs 46.02) (Table S1). This prompted us to explore if other parameters (*e.g.*, hydrogen bond donation and viscosity) also play a role. These parameters are known to affect the ϕ_F of merocyanine dyes, but not necessarily by modulating their electronic ground states.[42−46] Therefore, we conducted a systematic investigation of the photophysical (Figures 2A and S5A) and spectral properties (Figure S6) of **IndaFlav4** and **BarbiFlav4** in protic and aprotic solvents across a range of polarities (ϵ_R = 9.08−64.67) and viscosities (η = 0.43−7.36 cP) (Table S1).

We began our investigation into the ground state sensitivity of **IndaFlav4** (Figure 2B) and **BarbiFlav4** (Figure S5B) with solvent polarity. To minimize the influence of hydrogen bond donation and viscosity, we selected DCM and acetonitrile

https://doi.org/10.1021/acs.analchem.4c06185
Anal. Chem. 2025, 97, 5595−5604

(MeCN) as aprotic solvents with similar viscosities (η = 0.43 cP vs 0.34 cP), but different dielectric constants (ϵ_R = 9.08 vs 37.50). In the case of both **IndaFlav4** and **BarbiFlav4**, we observed minimal changes in their absorption spectra ($\Delta FWHM_{IndaFlav4}$ = 4 nm), suggesting that solvent polarity has a small impact on their ground states. Next, we determined the effects of viscosity using MeCN and *N*,*N*-dimethylformamide (DMF) as aprotic solvents with the same dielectric constant (ϵ_R = 37.50), but different viscosity values (η = 0.34 cP vs 0.92 cP). Both **IndaFlav4** and **BarbiFlav4** exhibit increasing cyanine character with increasing solvent viscosity ($\Delta FWHM_{IndaFlav4}$ = 19 nm). We observed a similar trend using the traditional glycerol titrations in MeOH[42,44−46] ($\Delta FWHM_{IndaFlav4}$ = 38 nm from 0 to 75% glycerol) (Figure S7), further supporting our hypothesis that viscosity is an influential parameter on the ground states of flavylium merocyanine dyes. Finally, to elucidate the role of hydrogen bonding, we selected MeOH and MeCN because they have similar dielectric constants (ϵ_R = 32.63 vs 37.50) and viscosity values (η = 0.55 cP vs 0.34 cP), but different hydrogen bonding abilities. In the case of both **IndaFlav4** and **BarbiFlav4**, we observed substantial increases in cyanine character ($\Delta FWHM_{IndaFlav4}$ = 57 nm), suggesting that hydrogen bond donation plays a very important role in stabilizing the cyanine ground state.

Since **IndaFlav4** and **BarbiFlav4** are sensitive to both viscosity and hydrogen bonding, we hypothesized that they would exhibit even stronger cyanine character in solvents with high degrees of both properties (Figures 2C and S5C). To test this hypothesis, we prepared aqueous mixtures of 25% water/MeCN and 25% water/DMSO, which have higher viscosities (η = 0.92 cP and 3.68 cP) than MeCN and DMSO alone, and are able to act as hydrogen bond donors. Going from pure MeCN to a 25% water/MeCN, we observed a remarkable increase in cyanine character for both **IndaFlav4** ($\Delta FWHM_{IndaFlav4}$ = 52 nm) and **BarbiFlav4**, with FWHM values on par to those in MeOH. This increase is even stronger going from pure DMSO to 25% water/DMSO ($\Delta FWHM_{IndaFlav4}$ = 56 nm), with each dye exhibiting the smallest FWHM of all eight solvents in these conditions. These results are especially gratifying in the context of biological investigations, as the presence of water is capable of inducing dramatic shifts toward the cyanine state. However, there are also many hydrophobic compartments within a biological setting (*e.g.*, organelle membranes, lipid droplets and protein cavities) where interactions with water are minimal. With this in mind, we examined the ground state properties of each dye in 1-octanol, a cell membrane mimic with low polarity (ϵ_R = 10.34), high viscosity (η = 7.36 cP), and the ability to hydrogen bond donate. On the basis of polarity, we would expect each dye to favor the polyene state, with absorption profiles similar to DCM. Instead, **IndaFlav4** and **BarbiFlav4** exhibit more cyanine character ($\Delta FWHM_{IndaFlav4}$ = 40 nm) which we attribute to contributions from viscosity and hydrogen bond donation. Although aqueous environments aid in favoring the cyanine state, these results demonstrate that hydrophobic environments with high viscosity and hydrogen bond donation can also favor the cyanine state of flavylium merocyanine dyes, increasing their utility across a range of biological settings.

Because we observed similar ground state properties for **IndaFlav4** and **BarbiFlav4**, we reasoned that the architecture of the flavylium donor (as opposed to the acceptor groups) is responsible for the pronounced solvent sensitivity. Based on previous work with cationic flavylium polymethine dyes,[47] we expect the decreased rotation of the phenyl substituent to increase the planarity of the fluorophore, leading to more efficient charge transfer and increased electron delocalization in viscous solvents. It remains unclear why there is increased cyanine character in protic solvents, but hydrogen bond donation presumably occurs with the acceptor end of the fluorophore, making this interaction applicable to other merocyanine dyes. To probe the contributions from the flavylium heterocycle, we prepared the previously reported indolenium analogs of each dye, which we named **IndaIndol4** (Figure 2D) and **BarbiIndol4** (Figure S6D). We expected the indolenium analogs to show less sensitivity to changes in viscosity because they do not contain the pendant aryl ring, but similar changes to hydrogen bonding, as that interaction is dependent on the acceptor. Surprisingly, both analogs exhibit minimal ground state changes across all eight solvents (Tables S2 and S3), with the largest ΔFWHM totaling only 10 nm for **IndaIndol4**. We attribute this to the fact that both dyes are very close to the cyanine state (indicated by their exceptionally narrow absorption spectra), making them less sensitive to solvent changes in general.[45] That being said, **IndaIndol4** exhibits slightly broader absorption in 1-octanol compared to other solvents, which is consistent with our hypothesis that contributions from solvent viscosity are less important for the indolenium scaffold. Additionally, the FWHM is smaller in solvents where strong hydrogen bond donation is possible, suggesting that this interaction is applicable to other merocyanine scaffolds. Overall, these data indicate that ground state sensitivity toward solvent viscosity is imparted by the structural makeup of the flavylium heterocycle.

Fluorescent Properties. After investigating their ground state properties, we then measured the fluorescence and ϕ_F of **IndaFlav4** (Figure 3A) and **BarbiFlav4** (Figure S8A) across all eight solvents. In the case of **IndaFlav4**, we were delighted to see NIR fluorescence spanning 720−738 nm and ϕ_F up to 16% depending on the solvent. The emission for **BarbiFlav4** is *ca.* 30 nm blue-shifted (690−715 nm), but still reaches the NIR region in certain solvents, with ϕ_F up to 18.8%. Considering the ground state sensitivity of flavylium merocyanine dyes, we were interested to see if there are any solvent parameters that affect their ϕ_F. Scaffolds between the A1—A2 ground states typically exhibit higher ϕ_F with increasing solvent polarity because they are approaching the more-emissive cyanine state. It has also been demonstrated that high solvent polarity minimizes the competing pathway of photoisomerization, leading to higher ϕ_F in these conditions.[48] In the case of **IndaFlav4** and **BarbiFlav4**, we noticed a general increase in ϕ_F with increasing solvent polarity, but their relatively high ϕ_F in 1-octanol led us to consider viscosity as another important solvent parameter. Polymethine dyes typically show enhanced ϕ_F in viscous solvents due to the suppression of molecular rotation and photoisomerization, potentially explaining why both dyes have high ϕ_F in 1-octanol, despite its low polarity.[49,50] Contributions from both solvent parameters can be analyzed on a three-dimensional bar graph that shows ϕ_F with respect to the increasing polarity and viscosity (Figures 3B and S8B). For both **IndaFlav4** and **BarbiFlav4**, there is a pronounced ϕ_F enhancement with increasing polarity and viscosity, suggesting that the additive effect of each parameter is important for suppressing alternative pathways of nonradiative decay.

https://doi.org/10.1021/acs.analchem.4c06185
Anal. Chem. 2025, 97, 5595−5604

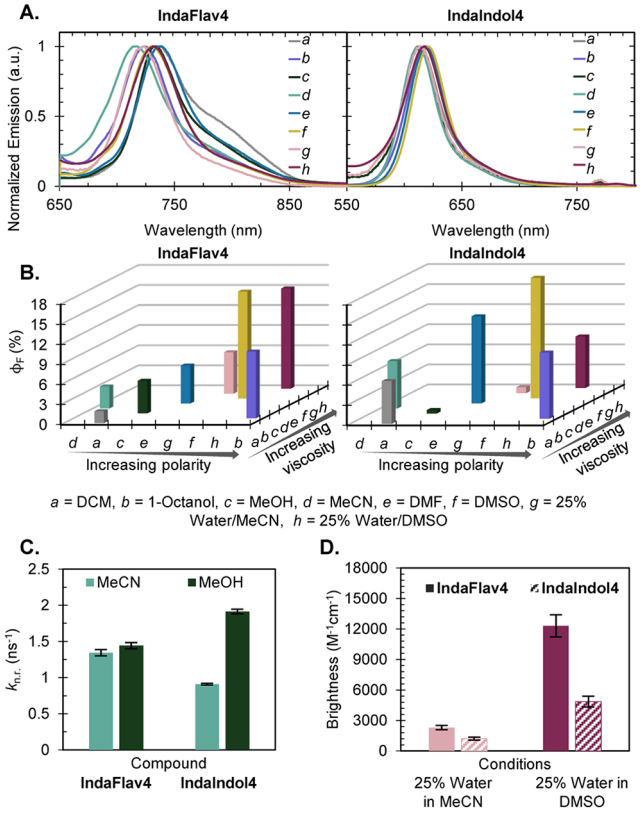

Figure 3. Fluorescent properties of **IndaFlav4** and **IndaIndol4** in various solvents. (A) Normalized fluorescence spectra of **IndaFlav4** (12 μM, ex. 620 nm; collect 650−900 nm) and **IndaIndol4** (3.0 μM, ex. 510 nm; collect 550−900 nm) in various solvents. (B) Three-dimensional bar graphs of the ϕ_F for **IndaFlav4** and **IndaIndol4** with increasing solvent viscosity and polarity. (C) Bar graph of the calculated rates of nonradiative decay ($k_{n.r.}$) for **IndaFlav4** and **IndaIndol4** in MeCN and MeOH. Error bars represent the standard deviation of three replicates. (D) Bar graphs of the calculated brightness ($\epsilon \times \phi_F$) for **IndaFlav4** and **IndaIndol4** in various solvents. Error bars represent the propagated error of ϵ and ϕ_F.

To determine if this behavior is unique to the flavylium scaffold, we investigated the emission and ϕ_F of the indolenium merocyanine dyes across all eight solvents. As expected, both dyes display blue-shifted emission spanning 612−621 nm for **IndaIndol4** (Figure 3A) and 585−593 nm for **BarbiIndol4** (Figure S8A). Furthermore, their ϕ_F values are generally higher ($\phi_F \leq 18\%$ for **IndaIndol4** and $\leq$50% for **BarbiIndol4**) than the flavylium merocyanine dyes, likely due to the absence of the pendant aryl ring. Interestingly, the indolenium analogs show a stronger relationship between ϕ_F and solvent viscosity than polarity (Figures 3B and S8B). Again, the indolenium heterocycle does not have the pendant aryl ring, so molecular rotation should be less of a competing pathway for nonradiative decay. Instead, these results may derive from the propensity for indolenium polymethine dyes to undergo photoisomerization, which gets suppressed in viscous solvents like 1-octanol.[45,48]

Another notable comparison between the flavylium scaffold and the indolenium scaffold is their sensitivity to protic solvents, particularly in the case of the 1,3-indandione analogs. Quenched fluorescence in protic solvents has been reported for this class of acceptors, caused by hydrogen bond-induced stabilization of the charge-transfer excited state, which then rapidly relaxes via nonradiative decay.[51−53] Consequently, **IndaIndol4** is essentially nonfluorescent in MeOH (ϕ_F = 0.54%) and 25% water/MeCN (ϕ_F = 0.9%), and only recovers fluorescence in solvents with higher viscosity like 1-octanol (ϕ_F = 9.9%) and 25% water/DMSO (ϕ_F = 7.7%). We noticed similar behavior for **IndaFlav4**, but the ϕ_F in MeOH (4.9%) and 25% water/MeCN (6.2%) are much higher relative to the ϕ_F in 1-octanol (10%) and 25% water/DMSO (16%), suggesting that the flavylium scaffold is more resistant to hydrogen bond-induced quenching. To evaluate the effect of hydrogen bond donation on the excited states of **IndaFlav4** and **IndaIndol4**, we conducted time-correlated single photon counting lifetime measurements in MeCN and MeOH to determine their rates of nonradiative decay ($k_{n.r.}$) (Figure 3C). Again, we selected these solvents to normalize for contributions from polarity and viscosity. In the case of **IndaFlav4**, we observed a marginal increase in the rate of nonradiative decay going from MeCN ($k_{n.r.}$ = 1.34 ns^{-1}) to MeOH ($k_{n.r.}$ = 1.44 ns^{-1}), suggesting that hydrogen bond donation plays a minor role in excited state deactivation. In contrast, we observed a 2-fold increase in the rate of nonradiative decay for **IndaIndol4** ($k_{n.r.}$ = 0.91 ns^{-1} in MeCN vs 1.9 ns^{-1} in MeOH), supporting our hypothesis that the indolenium scaffold is more susceptible to hydrogen bond-induced quenching than the flavylium scaffold. This could be attributed to the fact that **IndaFlav4**, as a weaker donor−acceptor pair, has less charge-transfer character in the excited state and therefore less hydrogen bond-induced stabilization. Overall, it is gratifying to see that in aqueous mixtures, both **IndaFlav4** (Figure 3D) and **BarbiFlav4** (Figure S8C) actually outperform their indolenium analogs in terms of ϕ_F and overall brightness ($\epsilon \times \phi_F$).

Intrinsic Labeling of the Endoplasmic Reticulum. Having achieved far-red flavylium merocyanine dyes that favor the cyanine state in biologically relevant conditions, we were eager to evaluate the utility of the most red-shifted dye, **IndaFlav4**, for live cell labeling. First, we assessed its cytotoxicity in A375 cells using a trypan blue exclusion assay at concentrations spanning 0−50 μM. We observed excellent cell viability (>96%) at concentrations up to 50 μM (Figure S9). Next, we tested its stability in 10 μM mixtures of hydrogen peroxide (H_2O_2), peroxynitrite ($ONOO^-$) and hydrogen sulfide (H_2S) (Figure S10,A) to determine if **IndaFlav4** can withstand reactive oxygen (ROS), nitrogen (RNS) and sulfur (RSS) species in cells. In all three conditions, characteristic absorption and emission of **IndaFlav4** is present after 2 h, suggesting adequate stability for use alongside the nanomolar concentrations of ROS, RNS, and RSS present in cells. We performed additional stability assessments in mixtures of citrate phosphate buffer at biologically relevant pHs 5.0, 6.0, and 7.4 (Figure S10,B). We were pleased to find that **IndaFlav4** retains strong absorption and emission after 12 h, indicating it is applicable for imaging acidic environments like the endosome and lysosome. After analyzing the chemical stability of **IndaFlav4**, we examined its photostability in 1-octanol with continual LED irradiation at 660 nm for 8 h (Figure S11). Remarkably, **IndaFlav4** showed only ∼15% absorption loss after 8 h, demonstrating its strong resistance toward photodegradation.

Upon confirming that **IndaFlav4** is biocompatible and stable, we performed confocal microscopy in living A375 cells (Figure 4). Because of its red-shifted absorption, **IndaFlav4** is efficiently excited with far-red laser lines, enhancing its

https://doi.org/10.1021/acs.analchem.4c06185
Anal. Chem. 2025, 97, 5595−5604

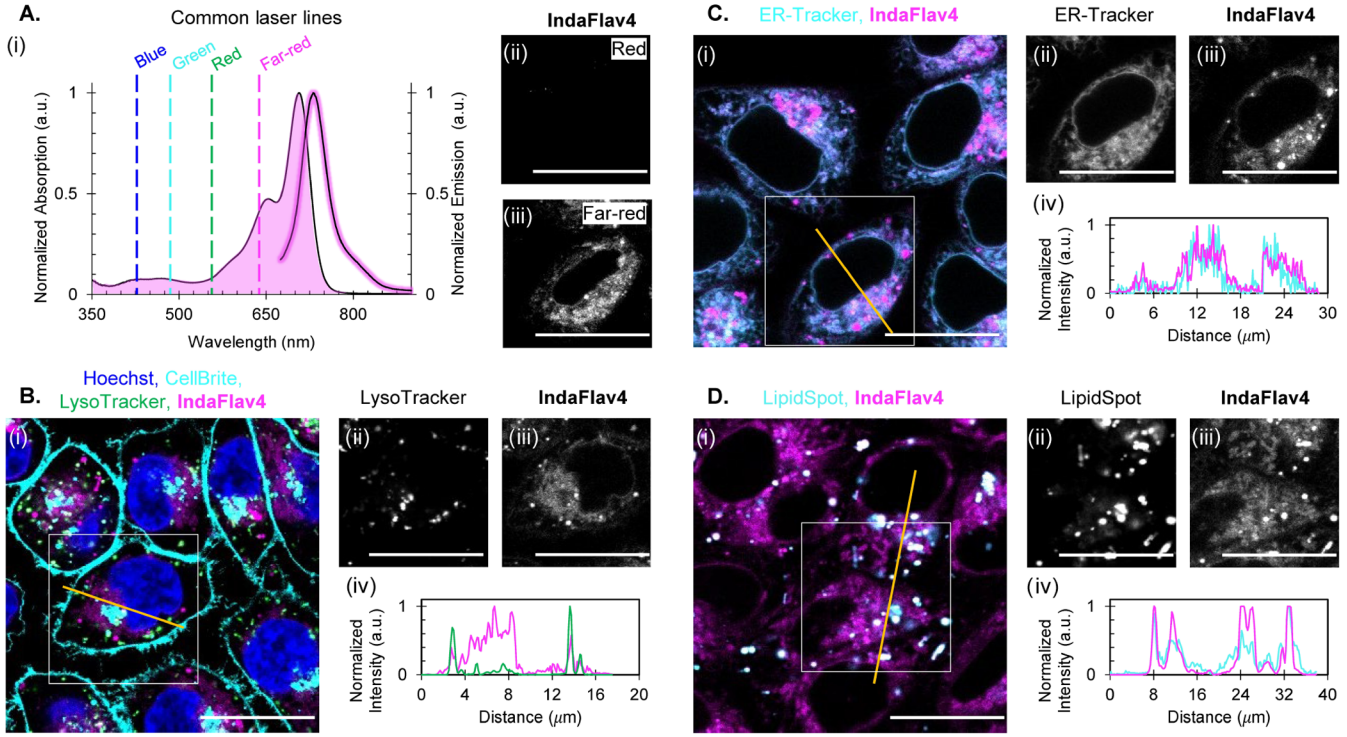

Figure 4. Live cell labeling with **IndaFlav4.** (A) Absorption and fluorescence profile of **IndaFlav4** plotted against common microscopy laser lines (i). Live cell confocal microscopy of A375 cells labeled with **IndaFlav4** (25 μM) and excited by a red laser line (ii, ex. 561 nm; collect 680−850 nm) and a far-red laser line (ii, ex. 638 nm; collect 680−850 nm). (B) Four-color confocal microscopy of live A375 cells labeled with Hoechst 33342 (i, blue, nucleus, ex. 405 nm; collect 420−470 nm), CellBrite Fix 488 (i, cyan, cell membrane, ex. 488 nm, 500−600 nm), LysoTracker Red DND-99 (i, green, lysosomes, ex. 561 nm; collect 575−651 nm) and **IndaFlav4** (i, magenta, 5 μM endoplasmic reticulum, ex. 638 nm; collect 680−800 nm). Zoomed inset (white box) of LysoTracker Red DND-99 (ii) and **IndaFlav4** (iii). Normalized cross-section analysis (yellow line) of LysoTracker Red DND-99 (iii, green) and **IndaFlav4** (iii, magenta). (C, D) Two-color confocal microscopy of live A375 cells labeled with ER-Tracker Green (C, i, cyan, endoplasmic reticulum, ex. 488 nm; collect 500−600 nm) or LipidSpot 488 (D, i, cyan, lipid droplets, ex. 488 nm; 500−600 nm) and **IndaFlav4** (C, D, i, magenta, 25 μM, ex. 638 nm; collect 680−850 nm). Zoomed inset (white box) of ER-Tracker Green (C, (ii)) or LipidSpot 488 (D, (ii)) and **IndaFlav4** (C, D, (iii)). Normalized cross-section analysis (yellow line) of ER-Tracker Green (C, iv, cyan) or LipidSpot 488 (D, iv, cyan) and **IndaFlav4** (C, D, iv, magenta). Scale bars represent 20 μm. The Pearson coefficient is 0.83 for the endoplasmic reticulum and 0.66 for lipid droplets.

compatibility with blue, green and red commercial stains and fluorescent proteins (Figure 4A). Capitalizing on this advantage, we performed a four-color colocalization experiment with **IndaFlav4** (Figure 4B,i, false color magenta) alongside conventional markers for the nucleus (Hoechst 33342, false color blue), cell membrane (CellBrite Fix 488, false color cyan) and lysosomes (LysoTracker Red-DND-99, false color green). Gratifyingly, we observed negligible crosstalk between LysoTracker Red and **IndaFlav4** (Figure 4B,iiii), highlighting its utility for multiplexed cell labeling. Additionally, we observed minimal colocalization with each cell marker (supported by cross-section analyses and Pearson coefficients less than 0.5), suggesting that **IndaFlav4** does not target the nucleus, cell membrane or lysosomes (Figures 4B,iv and S12). Based on its small size and moderate lipophilicity, we believe that **IndaFlav4** passively diffuses through the cell membrane, but is not lipophilic enough to be retained there.[54] Furthermore, its neutral charge is not ideal for DNA interactions in the nucleus or pH sensitivity in the lysosomes, resulting in poor localization to these organelles.[54] Lack of lysosomal staining also suggests that **IndaFlav4** is not internalized through the endosome, further supporting the notion that it is passively uptaken.[54]

Noticing the strong fluorescence surrounding the nucleus, we performed additional colocalization experiments for the mitochondria and endoplasmic reticulum (ER). Furthermore, the presence of bright puncta scattered throughout the cell prompted us to investigate if **IndaFlav4** labels lipid droplets, a known feature of some merocyanine scaffolds.[55−58] We observed minimal colocalization and dissimilar staining patterns to MitoTracker Green, suggesting that **IndaFlav4** does not target the mitochondria (Figure S12). This is not surprising considering cationic fluorophores are best suited for mitochondrial labeling.[54] In contrast, we observed excellent colocalization and similar staining patterns for ER-Tracker Green (Figure 4C) and LipidSpot 488 (Figure 4D), with respective Pearson coefficients of 0.83 and 0.66, confirming that **IndaFlav4** has intrinsic targeting ability to the ER and lipid droplets. This colocalization was maintained at a higher confocal resolution and magnification (Figure S13). To determine if this selectivity is present in other cell types, we labeled RAW264.7 macrophages with **IndaFlav4**, and observed excellent localization to both organelles (Figure S14).

The ER labeling achieved with **IndaFlav4** is a fortuitous discovery considering there are currently no commercial ER stains for excitation above 600 nm. We believe the intrinsic ER selectivity derives from the dipolarity achieved in the cyanine state and lipophilicity of the merocyanine architecture. It is well-established that ER-targeting fluorophores

https://doi.org/10.1021/acs.analchem.4c06185
Anal. Chem. 2025, 97, 5595−5604

should possess some amphiphilic character and sufficient lipophilicity, with calculated partition coefficients (Clog*P*) between 3.4 and 8.0.[59−63] The Clog*P* of **IndaFlav4** is 6.3, which is comfortably within this range (Table S4). We found that **BarbiFlav4** (Clog*P* = 5.6) and **IndaIndol4** (Clog*P* = 6.2) also localize to the ER (Pearson coefficients with ER Tracker Green = 0.82 and 0.86, respectively), supporting that this selectivity is related to the overall lipophilicity, rather than a particular structural motif (Figure S15). Most ER stains feature targeting groups (*e.g.*, bulky sulfonylurea ligands or ER-targeting peptides) that require additional synthetic steps and are known to disrupt cellular homeostasis.[59−64] In contrast, these merocyanine dyes are prepared in two high-yielding steps, and their simple design and low molecular weight impart excellent biocompatibility. We envision that, with careful tuning of their ground states and lipophilicity, merocyanine dyes possess unparalleled potential for future investigations of the endoplasmic reticulum.

CONCLUSIONS

In summary, we designed a new class of merocyanine dyes featuring a flavylium donor and a malononitrile (**Malono-Flav4**), 1,3-indandione (**IndaFlav4**) and *N*,*N*-dimethyl barbituric acid (**BarbiFlav4**) acceptor group. Capitalizing on the weak electron-donating properties of the flavylium heterocycle, all three dyes display red-shifted absorption spanning the far-red and NIR regions. Importantly, these dyes all lie between the A1—A2 ground states, depending on the acceptor strength and solvent properties.

We originally posited that these dyes favor the cyanine state with increasing polarity, as is typical with merocyanine dyes between the A1—A2 states, but ultimately discovered that the flavylium architecture imparts prominent sensitivity toward solvent viscosity. Therefore, these dyes exhibit pronounced cyanine character in high viscosity environments (*e.g.*, 1-octanol), regardless of polarity. We also found that merocyanine dyes featuring the 1,3-indandione and *N*,*N*-dimethyl barbituric acid acceptors favor the cyanine state in solvents with hydrogen bond donation, a phenomenon that has received no attention to date. This dual sensitivity toward viscosity and hydrogen bond donation allows flavylium merocyanine dyes to exhibit narrow, red-shifted absorption across a range of biologically relevant conditions, regardless of their polarity.

In addition to their unique ground state properties, we also discovered that **IndaFlav4** and **BarbiFlav4** exhibit higher ϕ_F with increasing solvent polarity and viscosity, a feature that is rarely seen in polymethine dyes. Furthermore, we demonstrate that **IndaFlav4** is more resistant to hydrogen bond-induced quenching compared to its indolenium analogue, improving the brightness of this scaffold in aqueous environments.

We exploit these properties for live cell microscopy, where we observed intrinsic targeting of both **IndaFlav4** and **BarbiFlav4** to the endoplasmic reticulum and lipid droplets. We attribute the intrinsic ER labeling to the dipolarity achieved in the cyanine state (which imbues subtle amphiphilic character) and lipophilicity ($C\log P$) of the merocyanine architecture. With access to a far-red scaffold between the A1—A2 ground states, we readily achieved four-color labeling with **IndaFlav4** alongside commercial stains, observing minimal crosstalk between detection windows. Having realized the potential of these flavylium merocyanine dyes for labeling experiments in cell culture, future work will involve extending their beneficial properties further into the NIR and shortwave infrared (SWIR, 1000−2000 nm) regions so we can further examine their utility in more complex biological settings.

ASSOCIATED CONTENT

Supporting Information

The Supporting Information is available free of charge at https://pubs.acs.org/doi/10.1021/acs.analchem.4c06185.

Figures S1-S15, Tables S1-S4, experimental procedures, and synthesis and characterization for all new compounds (PDF)

AUTHOR INFORMATION

Corresponding Author

Ellen M. Sletten − *Department of Chemistry and Biochemistry, University of California, Los Angeles, Los Angeles, California 90095, United States;* orcid.org/0000-0002-0049-7278; Email: sletten@chem.ucla.edu

Authors

Quintashia D. Wilson − *Department of Chemistry and Biochemistry, University of California, Los Angeles, Los Angeles, California 90095, United States;* orcid.org/0000-0001-5560-626X

Helen H. Lin − *Department of Chemistry and Biochemistry, University of California, Los Angeles, Los Angeles, California 90095, United States*

Eric Y. Lin − *Department of Chemistry and Biochemistry, University of California, Los Angeles, Los Angeles, California 90095, United States*

Lin-Jiun Chen − *Department of Chemistry and Biochemistry, University of California, Los Angeles, Los Angeles, California 90095, United States*

Complete contact information is available at: https://pubs.acs.org/10.1021/acs.analchem.4c06185

Author Contributions

Q.D.W. conceptualized the project, designed and executed the synthesis, performed the photophysical characterization/analysis, and wrote the manuscript. H.H.L. performed the microscopy and lifetime measurements. E.Y.L. performed the cell toxicity studies. L-J.C. assisted with the synthesis. E.M.S. supervised the project and acquired funding. Q.D.W., H.H.L., E.Y.L., and E.M.S. contributed to the revisions and editing of the final manuscript.

Notes

The authors declare no competing financial interest.

ACKNOWLEDGMENTS

This work was supported by UCLA (Cota-Robles Fellowship to Q.D.W.), the National Science Foundation (DGE-2034835 to H.H.L.), the Tobacco Related Disease Research Program (T32DT4847 to E.Y.L.), and the Chan Zuckerberg Initiative (2020-225707 to E.M.S.). We thank Prof. Alexander Spokoyny and the Advanced Light Microscopy and Spectroscopy Laboratory in CNSI at UCLA for use of their confocal microscopes, Joseph Garcia for acquiring a ^{19}F NMR and Dr. Diankai Lui for helpful discussions.

REFERENCES

(1) Lichtman, J. W.; Conchello, J.-A. *Nat. Methods* **2005**, *2* (12), 910−919.
(2) Fei, K.; Zhang, J.; Yuan, J.; Xiao, P. *Bioengineering* **2022**, *9* (3), No. 121.
(3) Lavis, L. D.; Raines, R. T. *ACS Chem. Biol.* **2014**, *9* (4), 855−866.
(4) Martin, A.; Rivera-Fuentes, P. *Nat. Chem.* **2024**, *16*, 28−35.
(5) Yuan, L.; Lin, W.; Zheng, K.; He, L.; Huang, W. *Chem. Soc. Rev.* **2013**, *42*, 622−661.
(6) Samanta, S.; Lai, K.; Wu, F.; Liu, Y.; Cai, S.; Yang, X.; Qu, J.; Yang, Z. *Chem. Soc. Rev.* **2023**, *52*, 7197−7261.
(7) Ishchenko, A. A. *Russ. Chem. Rev.* **1991**, *60*, 865−884.
(8) Bricks, J. L.; Kachkovskii, A. D.; Slominskii, Y. L.; Gera-sov, A. O.; Popov, S. V. *Dyes Pigm.* **2015**, *121*, 238−255.
(9) Gorka, A. P.; Nani, R. R.; Schnermann, M. J. *Org. Biomol. Chem.* **2015**, *13*, 7584−7598.
(10) Chen, X.; Li, J.; Roy, S.; Ullah, Z.; Gu, J.; Huang, H.; Yu, C.; Wang, X.; Wang, H.; Zhang, Y.; Guo, B. *Adv. Healthcare Mater.* **2024**, *13*, No. 2304506.
(11) Pascal, S.; David, S.; Andraud, C.; Maury, O. *Chem. Soc. Rev.* **2021**, *50*, 6613−6658.
(12) Chen, W.; Liu, T.; Zou, J.; Zhang, D.; Tse, M. K.; Tsang, S.-W.; Luo, J.; Jen, A. K.-Y. *Adv. Mater.* **2024**, *36* (17), No. 2306089.
(13) Bouit, P.-A.; Aronica, C.; Toupet, L.; Le Guennic, B.; Andraud, C.; Maury, O. *J. Am. Chem. Soc.* **2010**, *132*, 4328−4335.
(14) Pascal, S.; Haefele, A.; Monnereau, C.; Charaf-Eddin, A.; Jacquemin, D.; Le Guennic, B.; Andraud, C.; Maury, O. *J. Phys. Chem. A* **2014**, *118*, 4038−4047.
(15) Terenziani, F.; Przhonska, O. V.; Webster, S.; Padilha, L. A.; Slominsky, Y. L.; Davydenko, I. G.; Gerasov, A. O.; Kovtun, Y. P.; Shandura, M. P.; Kachkovski, A. D.; Hagan, D. J.; Van Stryland, E. W.; Painelli, A. *J. Phys. Chem. Lett.* **2010**, *1*, 1800−1804.
(16) van der Wal, S.; Kuil, J.; Valentijn, A. R. P. M.; Van Leeuwen, F. W. B. *Dyes Pigm.* **2016**, *132*, 7−19.
(17) Luciano, M. P.; Crooke, S. N.; Nourian, S.; Dingle, I.; Nani, R. R.; Kline, G.; Patel, N. L.; Robinson, C. M.; Difilippantonio, S.; Kalen, J. D.; Finn, M. G.; Schnermann, M. J. *ACS Chem. Biol.* **2019**, *14*, 934−940.
(18) Wang, Y.; Weng, J.; Lin, J.; Ye, D.; Zhang, Y. *J. Am. Chem. Soc.* **2020**, *142*, 2787−2794.
(19) Li, D.-H.; Schreiber, C. L.; Smith, B. D. *Angew. Chem., Int. Ed.* **2020**, *59*, 12154−12161.
(20) Jia, S.; Lin, E. Y.; Mobley, E. B.; Lim, I.; Guo, L.; Kallepu, S.; Low, P. S.; Sletten, E. M. *Chem* **2023**, *9*, 3648−3665.
(21) Pascal, S.; Haefele, A.; Monnereau, C.; Charaf-Eddin, A.; Jacquemin, D.; Le Guennic, B.; Maury, O.; Andraud, C. In *On the Versatility of Electronic Structures in Polymethine Dyes*, Proceedings SPIE; SPIE, 2014.
(22) Tolbert, L. M.; Zhao, X. *J. Am. Chem. Soc.* **1997**, *119*, 3253−3258.
(23) Li, D.-H.; Smith, B. D. *J. Org. Chem.* **2022**, *87*, 5893−5903.
(24) Yang, J.; Wang, K.; Zheng, Y.; Piao, Y.; Wang, J.; Tang, J.; Shen, Y.; Zhou, Z. *Angew. Chem., Int. Ed.* **2022**, *61*, No. e202202128.
(25) Pengshung, M.; Cosco, E. D.; Zhang, Z.; Sletten, E. M. *Photochem. Photobiol.* **2022**, *98*, 303−310.
(26) Kulinich, V.; Ishchenko, A. A. *Chem. Rec.* **2024**, *24*, No. e202300262.
(27) Mustroph, H. *Phys. Sci. Rev.* **2022**, *7*, 143−158.
(28) Kulinich, A. V.; Ishchenko, A. A. *Russ. Chem. Rev.* **2009**, *78*, 141−164.
(29) Parthasarathy, V.; Pandey, R.; Stolte, M.; Ghosh, S.; Castet, F.; Würthner, F.; Das, P. K.; Blanchard-Desce, M. *Chem. - Eur. J.* **2015**, *21*, 14211−14217.
(30) Mustroph, H.; Mistol, J.; Senns, B.; Keil, D.; Findeisen, M.; Hennig, L. *Angew. Chem., Int. Ed.* **2009**, *48*, 8773−8775.
(31) Würthner, F.; Archetti, G.; Schmidt, R.; Kuball, H.-G. *Angew. Chem., Int. Ed.* **2008**, *47*, 4529−4532.
(32) Kulinich, A. V.; Derevyanko, N. A.; Ishchenko, A. A. *Russ. Chem. Bull.* **2005**, *54*, 2820−2830.
(33) Ishchenko, A. A.; Kulinich, A. V.; Bondarev, S. L.; Knyukshto, V. N. *Opt. Spectrosc.* **2008**, *104*, 57−68.
(34) Ishchenko, A. A.; Kulinich, A. V.; Bondarev, S. L.; Knyukshto, V. N. *Russ. J. Gen. Chem.* **2007**, *77* (10), 1787−1798.
(35) Kulinich, V.; Derevyanko, N. A.; Mikitenko, E. K.; Ishchenko, A. A. *J. Phys. Org. Chem.* **2011**, *24*, 732−742.
(36) Kulinich, A. V.; Mikitenko, E. K.; Ishchenko, A. A. *Opt. Spectrosc.* **2015**, *119*, 39−48.
(37) Kulinich, V.; Derevyanko, N. A.; Ishchenko, A. A. *Russ. J. Gen. Chem.* **2006**, *76*, 1441−1457.
(38) Cosco, E. D.; Caram, J. R.; Bruns, O. T.; Bruns, O. T.; Franke, D.; Franke, D.; Day, R. A.; Day, R. A.; Farr, E. P.; Farr, E. P.; Bawendi, M. G.; Bawendi, M. G.; Sletten, E. M. *Angew. Chem., Int. Ed.* **2017**, *56*, 13126−13129.
(39) Cosco, E. D.; Spearman, A. L.; Ramakrishnan, S.; Lingg, J. G. P.; Saccomano, M.; Pengshung, M.; Arus, B. A.; Wong, K. C. Y.; Glasl, S.; Ntziachristos, V.; Warmer, M.; McLaughlin, R. R.; Bruns, O. T.; Sletten, E. M. *Nat. Chem.* **2020**, *12*, 1123−1130.
(40) Klikar, M.; Jelínková, V.; Růžičková, Z.; Mikysek, T.; Pytela, O.; Ludwig, M.; Bureš, F. *Eur. J. Org. Chem.* **2017**, *2017*, 2764−2779.
(41) Haenle, J. C.; Bruchlos, K.; Ludwigs, S.; Köhn, A.; Laschat, S. *ChemPlusChem* **2017**, *82*, 1197−1210.
(42) Bai, Y.; Huang, Y.; Wan, W.; Jin, W.; Shen, D.; Lyu, H.; Zeng, L.; Liu, Y. *Chem. Commun.* **2021**, *57*, 13313−13316.
(43) Gao, D.; Li, A.; Guan, L.; Zhang, X.; Wan, L. Y. *Dyes Pigm.* **2016**, *129*, 163−173.
(44) Yan, J.-w.; Zhu, J.; Zhou, K.; Wang, J.; Tan, H.; Xu, Z.; Chen, S.; Lu, Y.; Cui, M.; Zhang, L. *Chem. Commun.* **2017**, *53*, 9910−9913.
(45) Toutchkine, A.; Kraynov, V.; Hahn, K. *J. Am. Chem. Soc.* **2003**, *125*, 4132−4145.
(46) Wu, W.-N.; Song, Y.-F.; Zhao, X.-L.; Wang, Y.; Fan, Y.-C.; Xu, Z.-H.; James, T. D. *J. Chem. Eng.* **2023**, *464*, No. 142553.
(47) Dang, Z.; Liu, X.; Du, Y.; Wang, Y.; Zhou, D.; Zhang, Y.; Zhu, S. *Adv. Mater.* **2023**, *35*, No. 2306773.
(48) Hoche, J.; Schulz, A.; Dietrich, L. M.; Humeniuk, A.; Stolte, M.; Schmidt, D.; Brixner, T.; Würthner, F.; Mitric, R. *Chem. Sci.* **2019**, *10*, 11013−11022.
(49) Levitus, M.; Ranjit, S. *Q. Rev. Biophys.* **2011**, *44*, 123−151.
(50) Lutsyk, P.; Piryatinski, Y.; Kachkovsky, O.; Verbitsky, A.; Rozhin, A. *J. Phys. Chem. A* **2017**, *121*, 8236−8246.
(51) Zhong, Y.; Chen, Y.; Feng, X.; Sun, Y.; Cui, S.; Li, X.; Jin, X.; Zhao, G. *J. Mol. Liq.* **2020**, *302*, No. 112562.
(52) Hossen, T.; Sahu, K. *J. Phys. Chem. A* **2018**, *122*, 2394−2400.
(53) Herbich, J.; Waluk, J.; Thummel, R. P.; Hung, C.-Y. *Photochem. Photobiol. A* **1994**, *80*, 157−160.
(54) Zhu, M.; Li, W.; Sun, L.; Lv, Z.; Yang, X.; Wang, Y. *Coord. Chem. Rev.* **2024**, *512*, 215893−215917.
(55) Collot, M.; Fam, T. K.; Ashokkumar, P.; Faklaris, O.; Galli, T.; Danglot, L.; Klymchenko, A. S. *J. Am. Chem. Soc.* **2018**, *140*, 5401−5411.
(56) Mukherjee, T.; Martinez-Sanchez, R. J.; Fam, K. T.; Bou, S.; Richert, L.; Garnier, D.; Mély, Y.; Kanvah, S.; Klymchenko, A. S.; Collot, M. *Mater. Chem. Front.* **2021**, *5*, 2459−2469.
(57) Wu, X.; Wang, X.; Li, Y.; Kong, F.; Xu, K.; Li, L.; Tang, B. *Anal. Chem.* **2022**, *94*, 4881−4888.
(58) Guo, S.; Li, C.; Lian, L.; Le, Z.; Ren, Y.; Liao, Y.-X.; Shen, J.; Hou, J.-T. *ACS Sens.* **2023**, *8*, 3882−3891.
(59) Fujisawa, T.; Tamura, Y.; Yasueda, K.; Kuwata, I.; Hamachi, I. *J. Am. Chem. Soc.* **2018**, *140*, 17060−17070.
(60) Colston, J.; Horobin, R.; Rashid-Doubell, F.; Pediani, J.; Johal, K. *Biotech. Histochem.* **2003**, *78*, 323−332.
(61) Knewtson, K. E.; Rane, D.; Peterson, B. R. *ACS Chem. Biol.* **2018**, *13*, 2595−2602.
(62) Phaniraj, S.; Gao, S.; Rane, D.; Peterson, B. R. *Dyes Pigm.* **2016**, *135*, 127−133.
(63) Meinig, J. M.; Fu, L.; Peterson, B. R. *Angew. Chem., Int. Ed.* **2015**, *54*, 9696−9699.

https://doi.org/10.1021/acs.analchem.4c06185
Anal. Chem. 2025, 97, 5595−5604

(64) Singh, D.; Rajput, D.; Kanvah, S. *Chem. Commun.* **2022**, *58*, 2413−2429.

https://doi.org/10.1021/acs.analchem.4c06185
Anal. Chem. 2025, 97, 5595−5604